sciendo
Transactions on Aerospace Research eISSN 2545-2835, VOL. 273, NO. 4/2023, 1-17
DOI: 10.2478/tar-2023-0019

AIRFOIL TONAL NOISE PREDICTION USING URANS

Witold Klimczyk* and **Adam Sieradzki**
Department of Aerodynamics, Łukasiewicz Research Network – Institute of Aviation,
al. Krakowska 110/114, 02-256 Warsaw, Poland

Abstract

To examine the feasibility of the laminar boundary layer (LBL), vortex shedding (VS) tonal noise modelling using unsteady Reynolds-averaged Navier–Stokes (URANS) was investigated for the non-symmetric S834 airfoil. A transition SST turbulence model was used to model the laminar-turbulent transition and its vital influence on the laminar bubble and hydrodynamic instabilities generation. The influence of turbulence on the unsteady vortex patterns was investigated. Hence, the hybrid aeroacoustic analysis with Lighthill analogy was conducted to obtain the acoustic pressure field. The approach allowed us to model hydrodynamic instabilities and the resulting VS tonal noise. The frequency of VS matched the experimental data, giving the same 1/3 octave tonal peak only for a limited freestream turbulence regime. The simplification of the present method did not allow us to model the aeroacoustic feedback loop, and resulted in lack of instabilities for higher freestream turbulence.

Keywords: airfoil tonal noise; aeroacoustics; CFD
Type of the work: original article

1. INTRODUCTION

The increasing importance of aerodynamic noise is a result of recent emergence of, amongst others, wind turbines and multirotor unmanned (and potentially manned) vehicles. Prospects for incorporation of multirotor transport in densely populated urban areas [1] require the effective solutions to mitigate the aerodynamic noise.

Whereas the propeller noise is typically addressed by analysis of thickness and loading constituents, the influence of airfoil shape and the related airfoil self-noise cannot be neglected.

Airfoil self-noise is typically divided into five types [2]:

- Turbulent boundary layer (TBL) trailing edge noise, where the noise is generated as turbulence passes over the trailing edge. This typically results in a broadband noise spectrum.
- Laminar boundary layer (LBL) vortex shedding (VS) instability noise, which occurs for low Reynolds number and low turbulence flows. Hydrodynamic instabilities generated on the laminar bubble develop vortices responsible for high levels of tonal noise, which is schematically depicted in Figure 1.

© 2023 Author(s). This work is licensed under a Creative Commons Attribution-NonCommercial-NoDerivatives 4.0 International License.
* Corresponding Author: witold.klimczyk@ilot.lukasiewicz.gov.pl
ARTICLE HISTORY **Received** 2022-11-22 **Revised** 2023-06-30 **Accepted** 2023-09-11

- Boundary layer separation (BLS), which generates noise due to shed turbulent vorticity. Increasing angle of attack shifts position of separation towards the leading edge, resulting in deep stall, which in turn generates low-frequency noise.
- Blunt trailing edge (BTE) noise is caused by VS behind the thick trailing edge.
- Tip vortex noise results from highly turbulent flow occurring near the tips of lifting blades or wings.

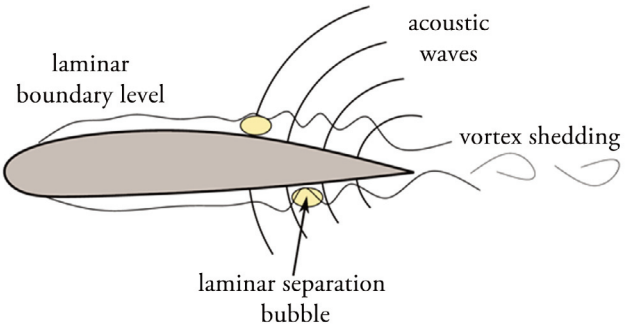


Figure 1. Mechanism of LBL, indicating VS noise generation.
LBL, Laminar boundary layer. VS, vortex shedding.

1.1. Airfoil tonal noise

One of the first comprehensive studies on airfoil tonal noise was an experimental research that was conducted in the 1970s [3]. The 'ladder-type' variation of the peak tone frequency f_S was obtained, relating it to the freestream flow speed u_∞, airfoil chord c and air kinematic viscosity $vf_s = 0.011u_\infty^{1.5}(cv)^{-0.5}$. The self-excited aeroacoustic feedback was soon proposed [4], which assumes that the tonal noise is due to the first instability excited by a point downstream. This idea was further investigated, so that the aeroacoustic signal was assumed to originate at the airfoil trailing edge as a result of Tollmien–Schlichting (T–S) waves diffraction. T–S waves are in turn triggered by the acoustic signal, which closes the feedback loop [5]. The validity of aeroacoustic feedback theory was discussed in the study of McAlpine et al. [6], and within that study it was concluded that the feedback is not necessary for the tonal noise to occur. It was found that the tonal noise is largely dependent on the existence of the separation bubble. In Lowson et al. [7], the authors established that the tones appear only up to a limited angle of incidence and in a certain Reynolds number range. Some more recent attempts can be found in Pröbsting et al. [8], which generally confirms the importance of the separation bubble in relation to the tonal noise and the tones' existence conditions.

In the light of these findings, LBL-VS is potentially important in the context of low Reynolds number propellers, which operate in low turbulence conditions and at moderate angles of attack [9]. Additionally, an appropriate computational model must be selected, which allows us to identify the existence of tonal noise on arbitrary airfoil, with the associated cost not ruling out the shape optimisation.

1.2. Computational aeroacoustics

The computational analysis of airfoil noise, especially if broadband noise is considered, requires a high-fidelity computational fluid dynamics (CFD) model, capable of resolving scales of turbulence, such as the large eddy simulation (LES) or hybrid RANS-LES [10]. The tonal nature of LBL-VS noise

requires appropriate modelling of laminar-TBL transition and formation of hydrodynamic instabilities, which propagate over the airfoil surface up to the trailing edge. Especially, late transition occurring at low turbulence conditions is important. The complexity of LBL-VS, further increased by the aeroacoustic feedback from the airfoil trailing edge, responsible for amplification of T–S waves, requires direct computational aeroacoustics (CAA) methods performed with direct numerical simulations (DNS) [11,12]. Whereas a direct application of CAA would resolve the acoustic field, the use of the relatively inexpensive unsteady Reynolds-averaged Navier–Stokes (RANS) model [13], in conjunction with the use of transition SST for turbulence closure, would suffice for modelling, with good accuracy, the existence of tonal noise as well as the levels of this noise. For the selected computational case of symmetric NACA airfoil, the method was shown whereby promising results, in agreement with the experiment described in the study of De Gennaro et al. [13], could be obtained. However, sufficient investigations have not been conducted regarding the performance associated with, as well as the limitations occurring in, a generic airfoil problem.

1.3. URANS modelling of airfoil tonal noise

In the present work, the validity of an incompressible unsteady Reynolds-averaged Navier–Stokes (URANS)-based modelling approach for airfoil LBL-VS tonal noise was assessed. The generic, asymmetric S834 airfoil was investigated, and the results obtained were compared to the experiment [14]. As the exact reproduction of an experimental setup, i.e. modelling the finite-span airfoil, was not feasible, the two-dimensional analysis of an airfoil, i.e. assuming an airfoil of infinite span, was conducted. The focus was thus on the qualitative aspects of tonal noise rather than the quantitative comparison of noise levels. Specifically, the existence and frequency of tones were of primary interest.

The present article is structured as follows: in Section 2, the details of aerodynamic and acoustic models are described. In Section 3, aerodynamic and acoustic results are presented and discussed. In Section 4, the summary and conclusions are stated.

2. AERODYNAMICS AND ACOUSTICS MODELLING

2.1. Aerodynamic model

Navier–Stokes (N–S) equations are used to describe the viscous fluid motion, which in the present instance is represented by the following continuity equation:

$$\frac{\partial \rho}{\partial t} + \nabla \cdot \left(\rho \vec{u} \right) = 0, \tag{1}$$

and the following momentum conservation equation:

$$\frac{\partial}{\partial t}\left(\rho \vec{u} \right) + \nabla \cdot \left(\rho \vec{u}\vec{u} \right) = -\nabla p + \nabla \cdot \left(\bar{\bar{\tau}} \right), \tag{2}$$

where p is the static pressure, ρ is the density, t is the time and $\bar{\bar{\tau}}$ is the stress tensor, defined as:

$$\bar{\bar{\tau}} = \mu \left[\left(\nabla \vec{u} + \nabla \overrightarrow{u^T} \right) - \frac{2}{3} \nabla \cdot \vec{u} I \right], \tag{3}$$

where μ is the molecular viscosity and I is the unit tensor.

So far as practical engineering applications are concerned, owing to the magnitude of the computational cost involved, derivation of direct numerical solutions to the N–S equations is not performed. The most popular simplification of N–S equations in industrial practice involves averaging; and among approaches involving averaging, the most popular, Reynolds averaging, gives RANS equations. RANS equations are of the form:

$$\frac{\partial}{\partial t}\left(\rho u_i\right)+\frac{\partial}{\partial x_j}\left(\rho u_i u_j\right)=-\frac{\partial p}{\partial x_i}+\frac{\partial}{\partial x_j}\left[\mu\left(\frac{\partial u_i}{\partial x_j}+\frac{\partial u_j}{\partial x_i}-\frac{2}{3}\delta_{ij}\frac{\partial u_k}{\partial x_k}\right)\right]+\frac{\partial}{\partial x_j}\left(-\rho u_i' u_j'\right) \tag{4}$$

where u represents the mean velocity and u' is the fluctuating term resulting from Reynolds averaging. Additional modelling of the fluctuating Reynolds stress term $\overline{-\rho u_i' u_j'}$ is required to close RANS equations. Eddy-viscosity models employ the Boussinesq hypothesis, which relates Reynolds stresses to the mean velocity gradients using the turbulent viscosity μ_T:

$$\overline{-\rho u_i' u_j'}=\mu_T\left(\frac{\partial u_i}{\partial x_j}+\frac{\partial u_j}{\partial x_i}\right)-\frac{2}{3}\left(\rho k+\mu_T\frac{\partial u_k}{\partial x_k}\right)\delta_{ij}. \tag{5}$$

The selection of eddy-viscosity model is case-specific. In this work, the requirement to accurately model the laminar bubble and the associated transition to the TBL led to the selection of a transition SST model [15], a common choice in the literature [16]. Transition SST is a four-equations, correlation-based turbulence model, which solves transport equations for turbulence kinetic energy k, specific dissipation rate ω, intermittency γ and momentum thickness Reynolds number Re_θ, which define the transition onset criteria. The model shows very good agreement with experiments and outperforms many other eddy-viscosity models in airfoil analysis requiring laminar-to-turbulent transition prediction [17].

In the present work, airfoil analysis at low Mach and moderate Reynolds number (Re) at the angle of attack (α) of 4° is considered. The case summary is presented in Table 1. In addition to the baseline case (u_∞ = 32 m/s), two additional analyses (u_∞ = 22.4 m/s and u_∞ = 47.9 m/s) are performed to confirm or refute the baseline conclusions.

Table 1. Case summary.

u_∞	22.4, 32, 47.9 [m/s]
ρ	1.225 [kg/m^3]
Re	5×10^5 [–]
α	4.4 [°]
c	0.2286 [m]
TI_{LE}	0.18%–0.99%

2.1.1. Computational domain and boundary conditions

The analyses were performed with a 2D model, which exploits the two-dimensional nature of LBL-VS and significantly reduces the computational cost. The domain extends over 20 chords upstream and almost 40 chords downstream from the airfoil. The problem was defined using common boundary conditions for incompressible flow, namely velocity-inlet with required freestream velocity and pressure-outlet in the downstream of domain (Fig. 2).

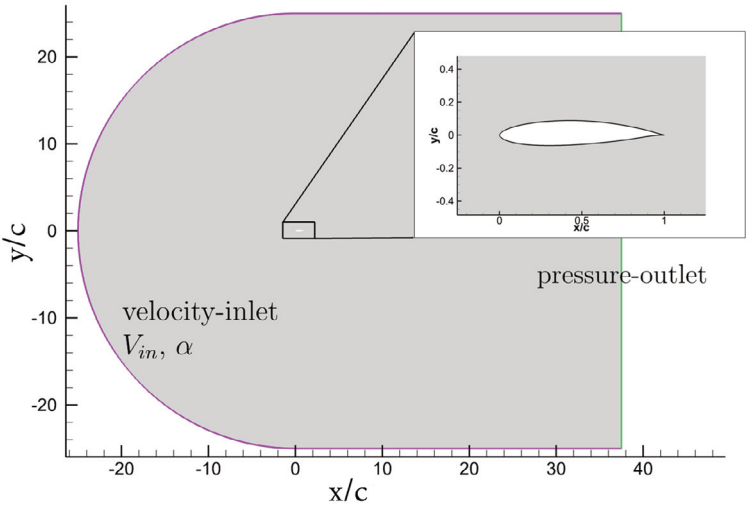


Figure 2. Computational domain schematic view with boundary conditions.

Due to the turbulence dissipation in the computational domain, its value is computed from the results of CFD model at the location directly above the leading edge of an airfoil. The turbulence at the inlet of the computational domain is controlled using the turbulence intensity and turbulent viscosity ratio.

Turbulence intensity is defined as:

$$\mathrm{TI} = \frac{u'}{U},$$

where u' is the root mean square of the turbulent velocity fluctuations:

$$u' = \sqrt{\frac{1}{3}\left(\overline{u_x'^2} + \overline{u_y'^2} + \overline{u_z'^2}\right)} = \sqrt{\frac{2}{3}k},$$

and U is the mean (Reynolds-averaged) velocity:

$$U = \sqrt{U_x^2 + U_y^2 + U_z^2}.$$

2.1.2. Mesh

The selected turbulence model (transition SST requires a mesh that allows resolution of the viscous sublayer, and specifically in such a way that y^+ does not exceed unity. The mesh is particularly important in the region of laminar-turbulent transition (laminar bubble), where the hydrodynamic instabilities are formed. Moreover, the region downstream of the laminar bubble should be well-modelled, such that the VS directly influencing pressure oscillations on the airfoil surface is properly resolved. A structured C-mesh was used to achieve orthogonal mesh in the region surrounding the airfoil (Fig. 3). The mesh consists of 305,000 quadrilateral elements. The near wall mesh is presented in Figure 4, whereas the mesh near the trailing edge is presented in Figure 5. The airfoil trailing edge is blunt, with three elements across its thickness.

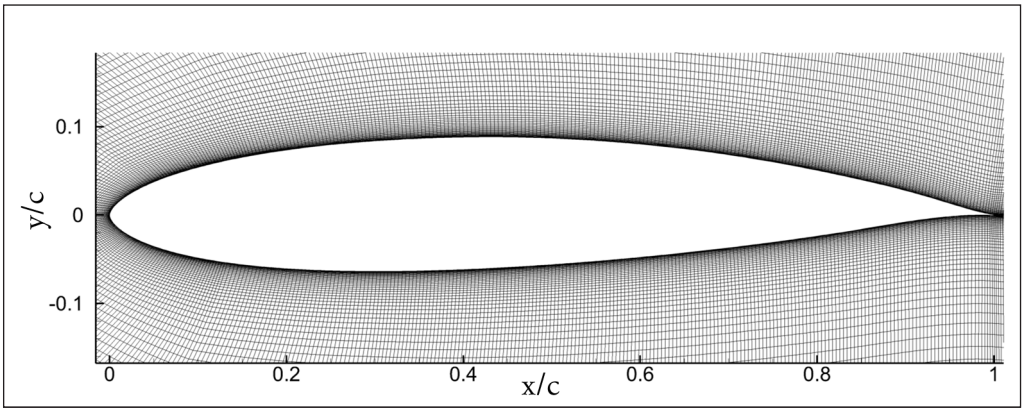


Figure 3. Mesh around the airfoil.

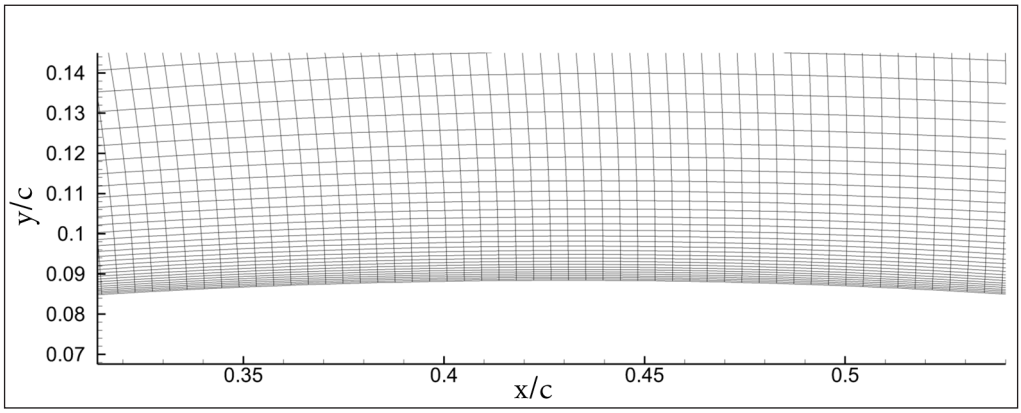


Figure 4. Mesh close up: maximum thickness of the near wall region at the airfoil.

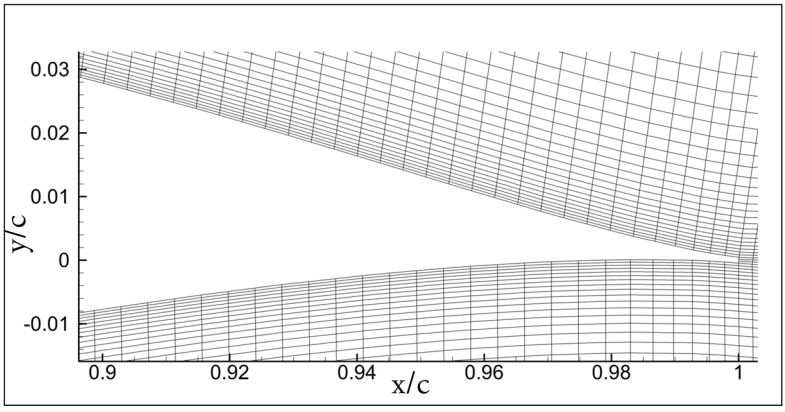


Figure 5. Mesh around the rear part of the airfoil.

2.1.3. CFD setup

In this work, a commercial software Ansys Fluent 21 [18] was used compute the flowfield around the airfoil. The incompressible pressure-based solver was selected due to low freestream velocity (u_∞ < 0.1 M). Firstly, a steady RANS solution was calculated using a coupled pressure–velocity solver. An unsteady solution was calculated starting from the steady RANS solution, with a non-iterative time advancement (NITA) fractional step scheme. A bounded second order implicit scheme was used for temporal discretisation. Least squares cell-based method was used to calculate gradients. To reduce the numerical dissipation, pressure was discretised using a second order scheme, whereas the second order upwind scheme was used for convection terms of the governing equations and the equations of turbulence model. The Courant–Friedrichs–Lewy (CFL) number was strictly below 1 everywhere in the domain, with maximum CFL ≃ 0.5 in the region of hydrodynamic instabilities formation, which resulted in the time step dt = 1×10^{-6} s. The turbulence intensity at the airfoil was controlled by setting the turbulence intensity and turbulent viscosity ratio (which affects the turbulence dissipation) at the inlet. The solution was calculated for 200,000 timesteps, which was sufficient to obtain a statistically converged solution. The computational time of a single case took approximately 24 h using 20 processes.

2.2. Aeroacoustics modelling using hybrid approach

The hybrid approach to modelling aeroacoustics is based on the separation of flow dynamics and acoustics. Firstly, the aerodynamic model is calculated. Then the noise sources are computed and propagated to the observer location using a selected method. The possible approaches include Curle analogy [19], Ffowcs Willimas–Hawkings analogy [20], Lighthill analogy [21,22], and others. The latter approach, schematically presented in Figure 6, is used in this work.

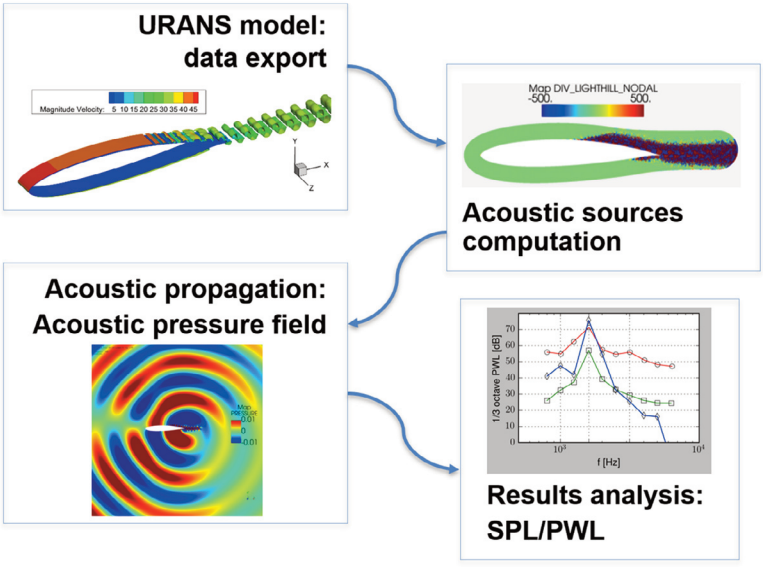


Figure 6. Aeroacoustics using hybrid approach with Lighthill analogy.
URANS, unsteady Reynolds-averaged Navier–Stokes.

Lighthill's analogy is formulated by rearranging N–S equations with acoustic density perturbation $\rho' = \rho - \rho_0$:

$$\frac{\partial^2 \rho'}{\partial t^2} - c_0 \frac{\partial^2 \rho'}{\partial x_i \partial x_i} = \frac{\partial^2 T_{ij}}{\partial x_i \partial x_j}, \tag{6}$$

where the left side of equation describes a propagation operator for all regions of the domain and the right side describes an equivalent acoustic source. It is described for source region only and is based on the Lighthill tensor T_i approximation for low Mach, incompressible flow, lending itself to expression as:

$$T_{ij} \approx \rho u_i u_j, \tag{7}$$

i.e. sources are calculated from velocity fluctuations. While the solution in the source region is typically discarded due to the limited accuracy, the calculated acoustic far-field is accurate. The Lighthill analogy can only be used under low freestream velocity conditions. It is based on the assumption that no acoustic sources are present in the far-field, which restricts the source region location. Important in the context of the present work is the separation of aerodynamics and acoustics. The model is unable to account for a potential aeroacoustic feedback unless the aerodynamic model captures it.

In the present work, Lighthill analogy, with volume sources in the region surrounding the airfoil, was used. The analysis was performed using a commercial software, *Actran 2021* [23]. To begin with, aeroacoustic sources were computed from the unsteady CFD results and transformed to the frequency domain. Thereafter, the finite element method-based solver was used to calculate the acoustic pressure propagation in the acoustic domain, with the corresponding mesh shown in Figure 7 (the yellow zone depicts the aeroacoustic source region). The mesh sizing was selected to allow modelling of frequencies between 300 Hz and 5,000 Hz, assuming at least six quadratic finite element (FE) cells per wavelength. The 1/3 octave band sound pressure levels were calculated at microphones surrounding the trailing edge at a distance of 0.63 m (as in the experiment).

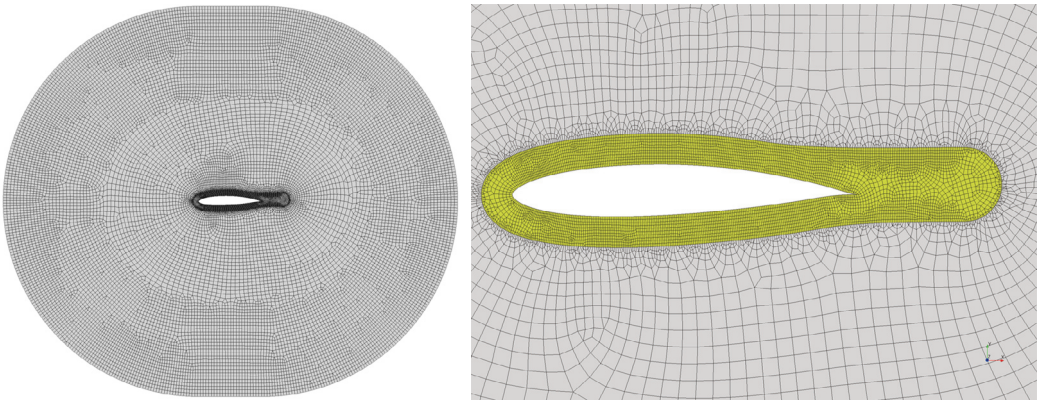


Figure 7. Acoustic FE mesh: domain (left) and close up to the airfoil (right).
Sources are calculated in the yellow zone and acoustic waves are propagated in the entire domain.

3. RESULTS AND DISCUSSION

3.1. Aerodynamics

To recreate the experimental environment, turbulence intensity not exceeding 1% had to be ensured at the airfoil [14]. However, the wind tunnel test section turbulence properties were not described in sufficient detail to allow more exact reproduction of the freestream conditions. For this reason, the influence of freestream turbulence, specifically turbulence intensity, on the computational model was investigated. In Figure 8, the example of turbulence dissipation is presented with turbulence intensity levels around the airfoil.

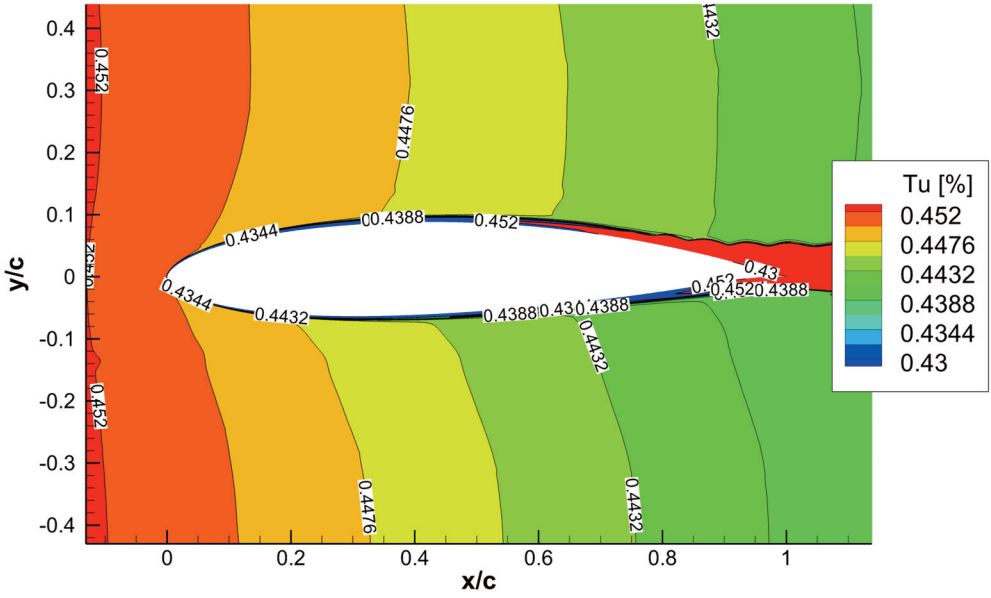


Figure 8. Turbulence intensity around the airfoil dissipated from 2% at the inlet.

Several analyses with turbulence intensity at the leading edge of an airfoil ranging from 0.18% to 0.99% were conducted. Figure 9 presents the instantaneous pressure coefficient on the rear part of the airfoil for turbulence intensities of 0.18% and 0.55%. The hydrodynamic instabilities are formed at the position of laminar bubble, approximately at 60% chord and 87% chord for the suction and pressure sides, respectively. Hence, on the suction side the pressure oscillations reach their maximum amplitude and begin to decay. On the pressure side, the oscillations are only observed for the lower turbulence case.

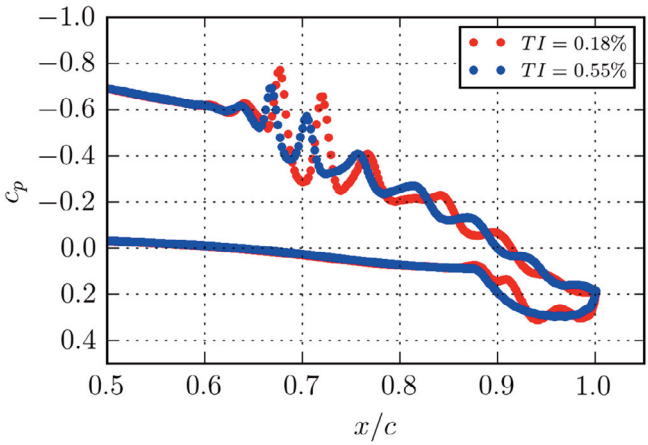


Figure 9. Instantaneous pressure coefficient at the rear part of the airfoil for different levels of turbulence.

A comparison of pressure contours for cases with different turbulence intensities is presented in Figure 10. Lower turbulence results in pressure oscillations at both pressure and suction sides, whereas for higher turbulence only suction side oscillations are present. It can be noted that the strength of vortices generated at suction side is higher for the lower turbulence (as assessed by density of the iso-pressure lines). Additionally, the vortices in the wake of an airfoil are only observed in the lower turbulence case.

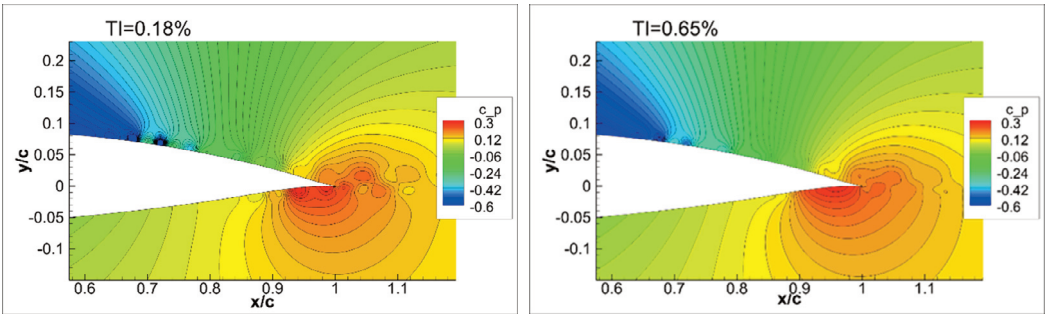


Figure 10. Pressure contours around the rear part of the airfoil for cases with 0.18% (left) and 0.65% (right) turbulence intensities.

The boundary layer in the vicinity of hydrodynamic instabilities formation is presented in Figure 11 for the low turbulence case (TI = 0.18%). The three snapshots were taken in equal time steps of 0.4 t_f, and time was scaled to match the period of suction side oscillations, i.e. $t_f = 1/f$. The centres of vortices were joined with lines to allow easy tracking of the vortices' movement. Initially, the vortices are very slow, as a result of which they are subject to acceleration, as can be observed from comparing the gradients of the joining lines.

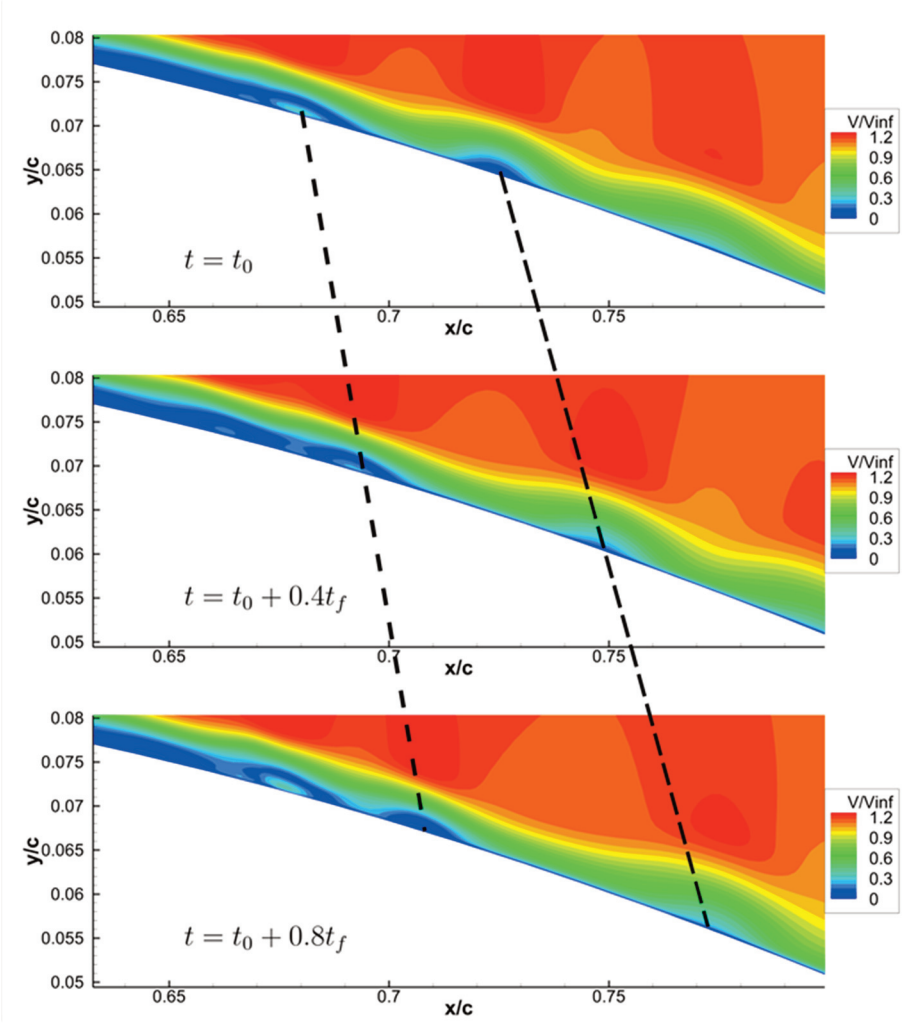


Figure 11. Snapshots of the formation of hydrodynamic instabilities in the boundary layer of S834 airfoil captured with URANS for TI = 0.18%. Lines join the vortical structures to help track their movement over the airfoil.

Similarly, in Figure 12, the vortices pattern is presented for the low turbulence case (TI = 0.18%), where the vortices are generated at both pressure and suction sides. The location and movement of these are visualised in the rear part of the airfoil using q-criterion. It can be observed that the vortex at the suction side, initially downstream of the pressure side vortex, is moving faster, and eventually passes the latter. Consequently, different frequencies of oscillations at both sides are expected to be observed during quantitative analysis.

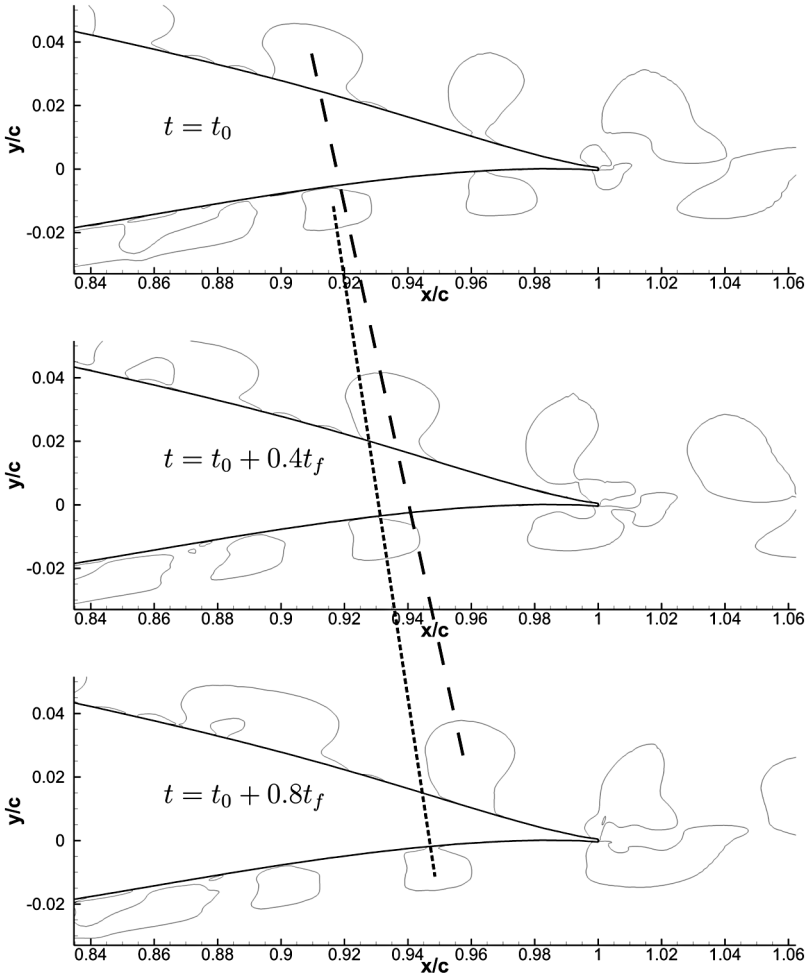


Figure 12. The vortical structures over pressure and suction sides of the airfoil as identified by q-criterion. The lines join vortices in three snapshots, showing the origin of different frequencies on both sides of the airfoil.

In Figure 13, drag monitor frequency domain representation is shown. Two peaks are observed: the major at f = 1,300 Hz corresponds to the frequency of oscillations at the pressure side and the secondary at f = 1,660 Hz corresponds to the frequency of oscillations at the suction side. Similar plots for remaining turbulence intensities show only single peak, corresponding to the suction side VS.

A summary of pressure oscillations' presence and strength is shown in Figure 14. The variation of peak amplitudes in spectral analysis of pressure signals, collected from four different points on the airfoil surface, is plotted against turbulence intensity. The general trend of decreasing amplitude with increasing turbulence intensity is observed. Vortices are only present on the pressure side for the lowest turbulence intensity case, while on the suction side they are observed up to the intensity of 0.65%. It should be noted that the amplitude of pressure oscillations on the suction side halves between the 87% chord and 96% chord locations, while on the pressure side the amplitudes are approximately doubled. In Table 2, a summary of peak tone frequencies and amplitudes for pressure signals collected at 87% chord and drag

counts (whole airfoil) is presented. An important result is shown for the case with a turbulence intensity of 0.18%, where the lower pressure amplitude at 1,300 Hz results in the peak frequency for drag signal. This result agrees with the generally observed dominant role of pressure side instabilities in the generation of tonal noise. For higher turbulence levels, where the pressure side oscillations are very small, their frequency is the same as that of the suction side oscillations, which suggests that these oscillations are generated by flow pattern of the suction side.

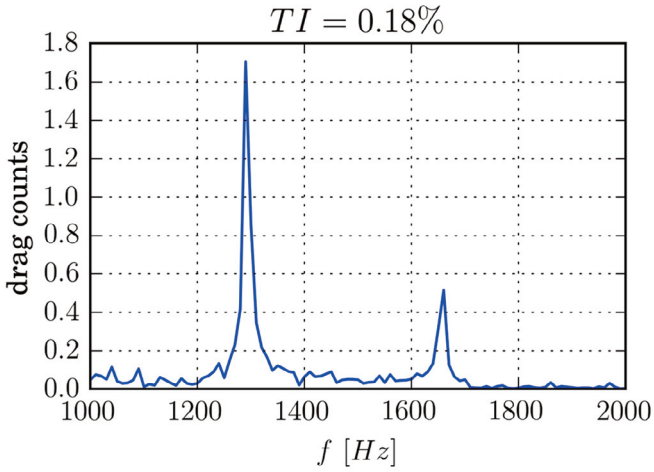


Figure 13. Frequency domain of drag monitor for the low turbulence case. The peak frequency of 1,300 Hz and secondary frequency of 1,660 Hz match the frequencies of pressure and suction side pressure oscillations.

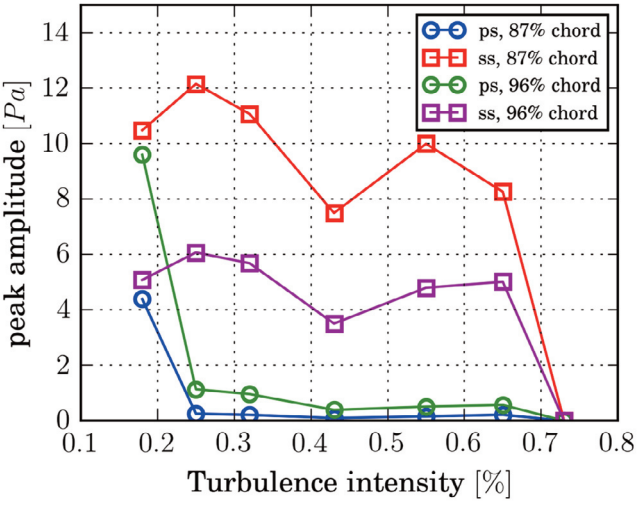


Figure 14. Summary of peak amplitudes of pressure fluctuations at two chord locations for the pressure side (ps) and the suction side (ss) depending on the turbulence intensity. Increasing turbulence affects pressure oscillations, which are only present at the lowest turbulence on the pressure side and disappear from the suction side at TI = 0.73%.

Table 2. Summary of peak tone frequencies and amplitudes for pressure signals collected at points at 96% chord and drag signal.

Turbulence Intensity	Suction side, 96% chord		Pressure side, 96% chord		Force (drag), airfoil	
	Frequency [Hz]	Amplitude [Pa]	Frequency [Hz]	Amplitude [Pa]	Frequency [Hz]	Amplitude (drag counts)
0.18%	1,660	5.1	1,300	9.6	1,300	1.7
0.25%	1,660	6.1	1,660	1.1	1,660	0.74
0.65%	1,620	5.0	1,620	0.6	1,620	0.66

The final assessment of the URANS modelling is performed by comparing the frequency and amplitude of drag oscillations for S834 airfoil at different freestream speeds, and thus different Reynolds numbers; a summary of the comparison results is presented in Table 3. It is observed that the frequency of oscillations for different Reynolds numbers is well-matched with the peak tone frequency measured in the experiment. These results were obtained at the turbulence intensities of 0.44% and 0.69% for freestream velocity values of 22.4 m/s and 47.9 m/s, respectively. Hence, the intensities were in the regime, where the expected LBL-VS frequency matches the experiment tonal noise peak, as shown for the baseline case. The trend of increasing sound power level (PWL) with increasing amplitude of drag oscillations is also maintained; however, due to various turbulence levels between cases, further conclusions cannot be drawn.

Table 3. Comparison of frequencies and amplitudes of drag oscillations for the baseline case (32 m/s) and additional cases at 22.4 m/s and 479 m/s, together with presentation of the experimental data pertaining to peak tone frequency (1/3 octave band centre) and PWL for comparison.

u_∞ [m/s]	TI	f_D [Hz]	Amplitude, drag counts	$f_{peak,\ EXP}$ [Hz]	PWL_{EXP} [dB]
22.4	0.44%	1,120	0.18	1,000	69.36
32.0	0.65%	1,620	0.74	1,600	71.32
47.9	0.69%	2,560	1.88	2,508	71.44

3.2. Acoustics

The acoustic pressure field is presented in Figure 15 for the frequency of 1,600 Hz. The following conclusions can be drawn:

1. The noise source is located at the trailing edge of an airfoil.
2. The hydrodynamic pressure oscillations appear at the laminar bubble and propagate downstream, over the trailing edge, and eventually form the wake. The wake does not contribute to the noise generation at the airfoil, and thus it is not required to participate in the calculation of aeroacoustic sources.
3. The directivity patterns can be clearly observed with higher and lower amplitudes of acoustic pressure.

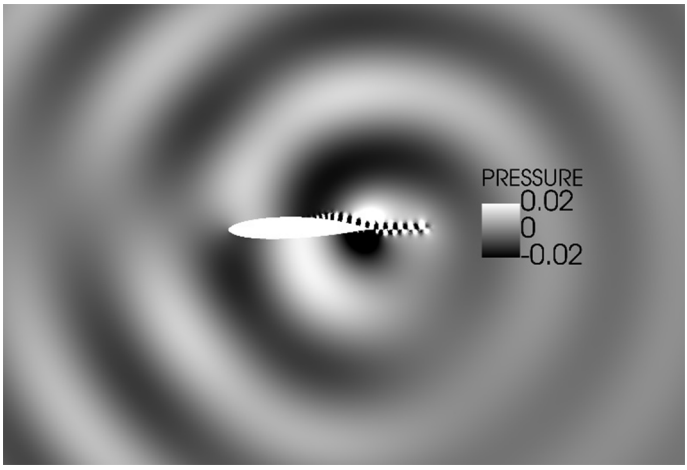


Figure 15. Acoustic pressure field around the airfoil (in Pascals) for the baseline case at the frequency of 1,600 Hz (i.e. the peak tone frequency). The origin of acoustic waves at the trailing edge is clearly visible, as is the directivity of emitted noise.

The quantitative comparison of noise levels obtained in the present work and in the experiment presented in the study of Oerlemans [14] is provided in Figure 16. The frequency of oscillations from the aerodynamic model was transferred to the noise tonal peak observed in the noise spectrum. The tone frequency from CAA matches the peak tone frequency measured in the experiment. The level of noise is, however, significantly higher than in the experiment. The difference can be attributed to the differences in the computational model setup, which assumes an ideal, infinite span airfoil, while the experiment was conducted on the finite wing. Noise levels' differences at the remaining frequencies result from turbulence averaging in RANS. To model higher frequencies scale resolving CFD is needed, which was not in the scope of the present work.

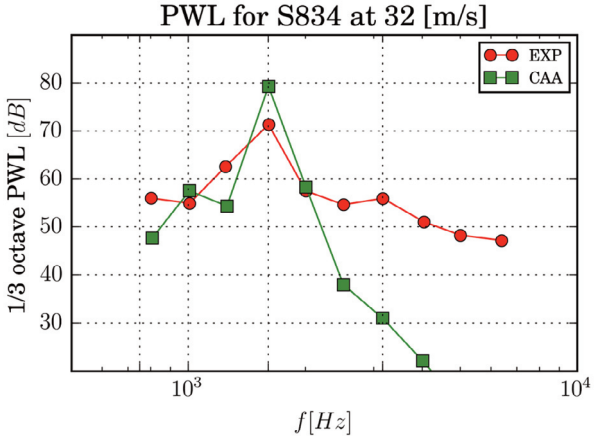


Figure 16. PWL from URANS and Lighthill analogy (CAA) compared to the experimental measurements (EXP). CAA, computational aeroacoustics; EXP, URANS, unsteady Reynolds-averaged Navier–Stokes.

SUMMARY

In this work, the feasibility of using low-cost URANS simulations to model the airfoil LBL-VS tonal noise was investigated. In comparison with the LES or DNS approaches, which are typically used in conjunction with direct application of CAA, the simplified physics model captured with URANS constitutes one of the important limitations characterising this approach. The lack of aeroacoustic feedback typically responsible for triggering the hydrodynamic instabilities resulted in a lack of these for cases calculated with a turbulence intensity just below 1%. On the other hand, for lower turbulence intensity, the laminar bubble was sufficient to form the instabilities, which propagated downstream, forming a VS pattern on the suction side. The frequency of oscillations at moderate turbulence intensity matched that of the experiment. At the lowest turbulence intensities, the oscillations appeared at the pressure side, and with a different frequency compared to those at the suction side. The resulting force oscillations' frequency was dominated by pressure side vortices, which represents a difference from the experimental results.

The main outcomes of this work are related to the sensitivity of analyses of LBL-VS to the freestream turbulence. The analyses showed a very significant sensitivity to freestream turbulence, with three different results within a 0%–1% turbulence intensity range: domination of pressure side vortices over suction side vortices (observed for TI = 0.18%), existence of suction side vortices only (observed for $0.25\% \leq TI \leq 0.65\%$) and lack of vortices for higher turbulence. Even though some of the results match the experimental measurements very well, the usefulness of URANS in the capturing of airfoil tonal noise remains limited.

Acknowledgements: This work has been supported by the Interdisciplinary Centre for Mathematical and Computational Modelling (ICM), University of Warsaw (UW), within grant No. G84-19.

REFERENCES

[1] Rizzi, S.A. "Urban Air Mobility Noise: Current Practice, Gaps, and Recommendations." No. NASA/TP-20205007433 (2020).

[2] Brooks, F., Pope, D., and Marcolini, A. *Airfoil Self-Noise and Prediction*, No. L-16528, NASA, 1989.

[3] Paterson, R.W., Vogt, P.G., Fink, M.R., and Munch, C.L. "Vortex Noise of Isolated Airfoils." Journal of Aircraft Vol. 10 No. 5 (1973): pp. 296–302.

[4] Tam, C.K.W. "Discrete Tones of Isolated Airfoils." *The Journal of the Acoustical Society of America* Vol. 55 No. 6 (1974): p. 5.

[5] Arbey, H. and Bataille, J. "Noise Generated by Airfoil Profiles Placed in a Uniform Laminar Flow." *Journal of Fluid Mechanics* Vol. 134 No. 1 (1983): p. 33.

[6] McAlpine, A., Nash, E.C., and Lowson, M.V. "On the Generation of Discrete Frequency Tones by the Flow around an Aerofoil." *Journal of Sound and Vibration* Vol. 222 No. 5 (1999): pp. 753–779.

[7] Lowson, M., Fiddes, S., and Nash, E. "Laminar Boundary Layer Aero-Acoustic Instabilities." *32nd Aerospace Sciences Meeting and Exhibi*. American Institute of Aeronautics and Astronautics. Reno, NV, U.S.A, 1994.

[8] Pröbsting, S., Serpieri, J., and Scarano, F. "Experimental Investigation of Aerofoil Tonal Noise Generation." *Journal of Fluid Mechanics* Vol. 747 (2014): pp. 656–687.

[9] Casalino, D., Grande, E., Romani, G., Ragni, D., and Avallone, F. "Definition of a Benchmark for Low Reynolds Number Propeller Aeroacoustics." *Aerospace Science and Technology* Vol. 113 (2021): p. 106707.

[10] Menter, F., Hüppe, A., Matyushenko, A., and Kolmogorov, D. "An Overview of Hybrid RANS–LES Models Developed for Industrial CFD." *Applied Sciences* Vol. 11 No. 6 (2021): p. 2459.

[11] Sandberg, R.D., Jones, L.E., Sandham, N.D., and Joseph, P.F. "Direct Numerical Simulations of Tonal Noise Generated by Laminar Flow Past Airfoils." *Journal of Sound and Vibration* Vol. 320 No. 4–5 (2009): pp. 838–858.

[12] Desquesnes, G., Terracol, M., and Sagaut, P. "Numerical Investigation of the Tone Noise Mechanism over Laminar Airfoils." *Journal of Fluid Mechanics* Vol. 591 (2007): pp. 155–182.

[13] De Gennaro, M., Kühnelt, H., and Zanon, A. "Numerical Prediction of the Tonal Airborne Noise for a NACA 0012 Aerofoil at Moderate Reynolds Number using a Transitional URANS Approach." *Archives of Acoustics* Vol. 42 No. 4 (2017): pp. 653–675.

[14] Oerlemans, S. *Wind Tunnel Aeroacoustic Tests of Six Airfoils for Use on Small Wind Turbines; Period of Performance: August 23, 2002 through March 31, 2004*, NREL/SR-500-35339, 15007773. 2004.

[15] Langtry, R.B. and Menter, F.R. "Correlation-Based Transition Modeling for Unstructured Parallelized Computational Fluid Dynamics Codes." *AIAA Journal* Vol. 47 No. 12 (2009): pp. 2894–2906.

[16] Dick, E. and Kubacki, S. "Transition Models for Turbomachinery Boundary Layer Flows: A Review." *International Journal of Turbomachinery, Propulsion and Power* Vol. 2 No. 2 (2017): p. 4.

[17] Rezaeiha, A., Montazeri, H., and Blocken, B. "On the Accuracy of Turbulence Models for CFD Simulations of Vertical Axis Wind Turbines." *Energy* Vol. 180 (2019): pp. 838–857.

[18] Ansys Inc. "Ansys Fluent, Release 21.1, Theory Guide", Canonsburg, Pennsylvania, USA, 2021.

[19] Curle, N. "The Influence of Solid Boundaries upon Aerodynamic Sound." *Proceedings of the Royal Society of London. Series A, Mathematical and Physical Sciences* Vol. 231 No. 1187 (1955): pp. 505–514.

[20] Ffowcs-Williams, J.E.F. and Hawkings, D.L. "Sound Generation by Turbulence and Surfaces in Arbitrary Motion." *Philosophical Transactions of the Royal Society of London. Series A, Mathematical and Physical Sciences* Vol. 264 No. 1151 (1969): pp. 321–342.

[21] Lighthill, M. "On Sound Generated Aerodynamically I. General Theory." *Proceedings of the Royal Society of London. Series A, Mathematical and Physical Sciences* Vol. 211 No. 1107 (1952): pp. 564–587.

[22] Lighthill, M. "On Sound Generated Aerodynamically. II. Turbulence as a Source of Sound." *Proceedings of the Royal Society of London. Series A, Mathematical and Physical Sciences* Vol. 222 No. 1148 (1954): pp. 1–32.

[23] Free Field Technologies SA. "ACTRAN VI 2021.1 User's Guide", Belgium, 2020.